We are IntechOpen,
the world's leading publisher of
Open Access books
Built by scientists, for scientists

4,400
Open access books available

117,000
International authors and editors

130M
Downloads

154
Countries delivered to

Our authors are among the

TOP 1%
most cited scientists

12.2%
Contributors from top 500 universities

BOOK CITATION INDEX
CLARIVATE ANALYTICS
INDEXED

WEB OF SCIENCE™

Selection of our books indexed in the Book Citation Index
in Web of Science™ Core Collection (BKCI)

Interested in publishing with us?
Contact book.department@intechopen.com

Long-Term Detection of Global Vegetation Phenology from Satellite Instruments

Xiaoyang Zhang[1], Mark A. Friedl[2], Bin Tan[3],
Mitchell D. Goldberg[4] and Yunyue Yu[5]

[1]Earth Resources Technology Inc. at NOAA/NESDIS/STAR, College Park,
[2]Department of Geography and Environment Boston University, Boston,
[3]Earth Resources Technology Inc. at NASA Goddard Space Flight Center, Greenbelt,
[4]NOAA/NESDIS/STAR, Camp Springs,
[5]NOAA/NESDIS/STAR, College Park,
USA

1. Introduction

Vegetation phenology is the expression of the seasonal cycles of plant processes and their connections to climate change (temperature and precipitation). The timing of phenological events can be used to document and evaluate the effects of climate change on both individual plant species and vegetation communities. Thus, vegetation phenology (including shifts in the timing of bud burst, leaf development, senescence, and growing season length) is considered as one of the simplest and most effective indicators of climate change (IPCC, 2007). Long-term observing and recording of changes in plant phenology support efforts to understand trends in regional and global climate changes, to reconstruct past climate variations, to explore the magnitude of climate change impacts on vegetation growth, and to predict biological responses to future climate scenarios.

Field phenological observations and calendars provide details of timing of seasonal development for specific plant species. The attributes of field phenophase observations include timing of flower bud or inflorescence appearance, first bloom, 50% bloom, end of blooming, fruit or seed maturing, fruit or seed shedding, first leaf unfolding, bud burst, 50% leaf unfolding, first leaf coloration, full leaf coloration, first defoliation, and end of defoliation. Such field observations have a history extending back for thousands of years in China (Zhu and Wan, 1963), and as far back as the early 1700s in Europe (e.g., Sparks and Carey, 1995), and the 1800s in Japan (Lauscher, 1978). Recently, several networks of field phenological observations have been established worldwide. The most notable of these networks are PlantWatch in Canada (http://www.naturewatch.ca/english/plantwatch/), the National Phenology Network (NPN, http://www.usanpn.org/) in the USA (United States of America), the European Phenology Network, the Japan Phenological Eyes Network (PEN, http://pen.agbi.tsukuba.ac.jp/), and the UK (United Kingdom) Phenology Network (http://www.phenology.org.uk/). The PlantWatch network is part of the Canadian national nature watch series of volunteer monitoring programs designed to help identify

ecological change. Plants chosen for the network are perennial, easy-to-identify, broadly-distributed, and naturally occurring species that bloom every spring in response to changing temperature. The European Phenology Network (EPN) involves various universities and research centers, and is supported by the International Society for Biometeorology, Commission on Vegetation Dynamics, Climate and Biodiversity. The USA NPN was established with support from USGS (US Geological Survey) in 2007, and is an interdisciplinary effort involving botanical gardens, academia, and government agencies, with the goal of systematically collecting and analyzing phenological data. This network observes phenology in about 2000 evenly distributed field sites across the USA.

An advanced technique for qualifying seasonality of plant canopy in the field is to take measurements using a digital webcam. The camera is generally mounted in a high tower (around 30 m tall) and is connected to a local wireless network and a personal computer running camera image-capture software (Richardson *et al.*, 2007). The imagery from digital cameras is capable of monitoring plant canopy seasonality (Richardson *et al.*, 2009), crop growth (Goddijn and White, 2006), and timing and duration of flowering (Adamsen *et al.*, 2000).

Long-term field observations of species-level phenophases have been successfully used to reveal local and regional climatic variations occurring for several decades (Fitter *et al.*, 1995; Kramer, 1996; Rötzer and Chmielewski, 2000; Chen *et al.*, 2005). Specifically, long-term records of budburst and flowering dates have been associated with inter-annual variation in air temperature. Previous studies revealed that warmer spring temperature has advanced flowering dates by about 4 days/°C (Fitter *et al.*, 1995) and leaf unfolding by about 3.2–3.6 days/°C in Europe (Kramer, 1996; Rötzer and Chmielewski, 2000). On average, springtime phenological events have changed globally by 2.3 days per decade (Parmesan and Yohe, 2003). Similarly, the growing-season length (GSL) of deciduous broadleaf forests during the period from 1900–1987 increased by about five days as a result of a one-degree increase in mean annual temperature in the eastern United States (White *et al.*, 1999). Moreover, phenological records have been used to model historical climate change. Indeed, the record of grape harvest dates for the period 1523–2007 in the area around Vienna, Austria, reveals that temperature was as warm in the 16th century as in the 1990s; the mean May to July temperature then started to fall, with the coldest decade of the record from 1771 to 1780; and a constant temperature increase from the 1970s to the present seems to be unprecedented during the last 470 years (Maurer *et al.*, 2009).

During the last three decades, remote sensing has become a widely-used mechanism for monitoring the activity of vegetation at large spatial scales. The satellite-derived vegetation indices, commonly termed normalized difference vegetation index (NDVI), provides an indication of the canopy "greenness" of vegetation communities, which is a composite property of leaf chlorophyll content, leaf area, canopy cover and structure. Therefore, the time series of NDVI data derived from the Advanced Very High Resolution Radiometer (AVHRR) have been used extensively for monitoring vegetation phenology (Lloyd, 1990; Reed *et al.*, 1994; White *et al.*, 1997; Zhang *et al.*, 2007). More recently, the VEGETATION instrument onboard the SPOT 4 spacecraft, and the Moderate Resolution Imaging Spectroradiometer (MODIS) onboard NASA's Terra and Aqua spacecraft, have provided a new era of global remote sensing observations. MODIS data produce time series of

vegetation indices at spatial resolutions of 250 m, 500 m, and 1 km globally, with substantially improved geometric and radiometric properties (Huete *et al.*, 2002).

Various phenology products have been developed from satellite data at regional and global scales. These products include: (1) the MODIS Land Cover Dynamics Product (MCD12Q2) derived from MODIS NBAR (nadir bidirectional reflectance distribution function adjusted reflectance) EVI (enhanced vegetation index) (500m–1000m), which is the only global product that is produced on an operational basis from 2001 to present (Zhang *et al*, 2006; Ganguly *et al*, 2010); (2) the MODIS-based product generated at NASA-GSFC (Goddard Space Flight Center) in support of the North American Carbon Program, which was produced using MODIS data at a spatial resolution of 250m–500m (Morisette *et al.*, 2009; Tan *et al.*, 2011); (3) the MODIS phenology product being generated for the contiguous United States (CONUS) by the US Forest Service (Hargrove *et al.*, 2009); (4) the USGS long-term 1-km AVHRR phenology product for CONUS (1989–present; Reed *et al.*, 1994); (5) the NOAA 4-km GVIx phenology over North America from 1982–2006 (Zhang *et al.*, 2007); (6) the global 4.6 km product for 2005 from the Medium Resolution Imaging Spectrometer (MERIS) Terrestrial Chlorophyll Index (MTCI) (Dash *et al.*, 2010); and (6) the global product based on FPAR (Fraction of Photosynthetically Active Radiation) developed by the European Space Agency (Verstraete *et al.*, 2008).

Satellite-derived phenology demonstrates recent climate change at a large spatial coverage. Using AVHRR NDVI between 1981 and 1991, Myneni *et al.* (1997) have estimated an advance of 8 ± 3 days in the onset of spring and an increase of 12 ±4 days in GSL in northern latitudes (45–70°N). An extended comparison of average AVHRR-NDVI values from July 1981 to December 1999 has shown that the duration of growing seasons increased by as much as 18 days in Europe and Asia, and by 12 days in northern North America (Zhou *et al.*, 2001). Furthermore, analysis of phenology derived from AVHRR NDVI between 1981 and 2006 across North America indicates that vegetation greenup onset advanced by 0.32 days/year in cold and temperate climate regions because of spring warming temperatures, while it changed progressively from an early trend (north region) to a later trend (south region) in subtropical regions because the shortened winter chilling days were insufficient to fulfill vegetation chilling requirements (Zhang *et al.*, 2007). However, little significant phenological trend has been found using the phenology detection capabilities of AVHRR NDVI during 1982–2006 over North America (White *et al.*, 2009).

Monitoring of vegetation phenology from remote sensing remains a significant challenge, although this technique has been demonstrated to be a robust tool. This is because satellite observations are frequently interfered with various abiotic factors, and a satellite footprint covers a large vegetation community at landscape scales. This chapter briefly introduces current methods in phenology detection from satellite data, and further presents long-term variation in satellite-derived vegetation phenology at the scale of global coverage.

2. Overview of phenology detection from satellite data

2.1 Vegetation index for phenology detection

Vegetation index (VI) derived from satellite data has been widely applied to monitor vegetation properties. The most commonly used vegetation index is the Normalized

Difference Vegetation Index (NDVI). It was first formulated by Rouse *et al.* (1973) using the following formula:

$$NDVI = \frac{\rho_{NIR} - \rho_{red}}{\rho_{NIR} + \rho_{red}} \qquad (1)$$

where ρ_{NIR} and ρ_{red} stand for the spectral reflectance measurements acquired in the near-infrared and red regions.

The NDVI derived from satellite data has been proved to be a robust tool for retrieving local and global vegetation properties, including vegetation type, net primary product, leaf area index, foliage cover, phenology, photosynthetically active radiation absorbed by a canopy (FPAR), evapotranspiration (ET), and biomass (e.g. Tucker *et al.*, 1986; Unganai and Kogan, 1998; Loveland *et al.*, 1999; Myneni *et al.*, 2002, Friedl *et al.*, 2002). More importantly, a long time series of AVHRR NDVI data has been widely applied for exploring global climate change reflected by variation of inter-annual vegetation phenology (Read *et al.*, 1994; Myneni *et al.*, 1997; Zhou *et al.*, 2001; Nemani *et al.*, 2003; Zhang *et al.*, 2007). Although NDVI provides researchers with a way to monitor vegetation characteristics, the use of NDVI across a variety of vegetation types may be limited by sensitivity to background reflectance (soil background brightness and moisture condition) (Huete *et al.*, 1985; Bausch, 1993), the attenuation caused by highly variable aerosols (Kaufman and Tanré, 1992; Miura *et al.*, 1998; Ben-Ze'ev *et al.*, 2006), and the saturation at densely vegetated areas (Huete *et al.*, 2002; Gitelson, 2004).

The enhanced vegetation index (EVI) has been developed to improve the quantification of vegetation activity (Huete *et al.*, 2002). EVI reduces sensitivity to soil and atmospheric effects, and remains sensitive to variation in canopy density where NDVI becomes saturated (Huete *et al.*, 2002). It is calculated from reflectance in blue, red and near-infrared bands, using the formula:

$$EVI = G \frac{\rho_{NIR} - \rho_{red}}{\rho_{NIR} + C_1\rho_{red} - C_2\rho_{blue} + L} \qquad (2)$$

where ρ_{blue}, ρ_{red} and ρ_{NIR} are values in the blue, red, and near-infrared bands, respectively, L (=1) is the canopy background adjustment, C_1 (=6) and C_2 (=7.5) are aerosol resistance coefficients, and G (=2.5) is a gain factor.

As described in the above equation, EVI requires information on reflectance in blue wavelengths, which is not available on some satellite instruments, including SPOTVGT, SeaWiFS, ENVISAT-MERIS, GLI, and AVHRR. To overcome this limitation, a two band EVI (EVI2) has been proposed (Huete *et al.*, 2006; Jiang *et al.*, 2008), which is described as:

$$EVI2 = G \frac{\rho_{NIR} - \rho_{red}}{\rho_{NIR} + C_3\rho_{red} + L} \qquad (3)$$

where C_3 is a coefficient (2.4).

The two-band adaptation of EVI2 is fully compatible with EVI (Huete *et al.*, 2006; Jiang *et al.*, 2007). The EVI2 remains functionally equivalent to the EVI, although slightly more prone to

aerosol noise, which is becoming less significant with continuing advancements in atmosphere correction. Similar to EVI, EVI2 is less sensitive to background reflectance, including bright soils and non-photosynthetically active vegetation (i.e. litter and woody tissues) (Rocha *et al.*, 2008). Thus, it could be used to monitor vegetation phenology and activity across a variety of ecosystems (Rocha and Shaver, 2009).

There are several other vegetation indices in vegetation phenology detections. These include Normalized Difference Water Index (NDWI) (Delbart *et al.*, 2005), FPAR (Verstraete *et al.*, 2008), and LAI (Obrist *et al.*, 2003).

2.2 Algorithm of phenology detection

Phenology detections from time series of satellite data are commonly composed of two steps: modeling of the temporal VI trajectory and identification of the timing of phenological phases. Modeling (or smoothing) of the temporal VI trajectory is to reduce non-vegetative information (noise) in the satellite observations. The noise in an annual time series is mainly caused by environmental impacts: cloud cover, atmospheric effects, and snow cover. To minimize cloud and atmospheric contamination, the maximum value composite (MVC) (Holben, 1986) and best index slope extraction (BISE) (Viovy *et al.*, 1992) are commonly applied to create weekly, biweekly, or monthly composites. To further reduce noise, time series of VI data are often smoothed using a variety of different methods including Fourier harmonic analysis (Moody and Johnson, 2001), asymmetric Gaussian function-fitting (Jonsson and Eklundh, 2002), piece-wise logistic functions (Zhang *et al.*, 2003), Savitzky–Golay filters (Chen *et al.*, 2004), degree-day based quadratic models (de Beurs and Henebry, 2004), and polynomial curve fitting (Bradley *et al.*, 2007). In mid- and high latitudes, vegetation signals are also contaminated by snow cover during winter. To reduce snow contamination, which generally results in a dramatically steep drop in NDVI and irregular variation in EVI (Zhang *et al.*, 2006), snow cover observations are explicitly removed or replaced. This is done using nearest non-snow observations in a temporal VI trajectory after winter periods are determined using ancillary data of land surface temperature and snow detection (Zhang *et al.*, 2004a; Tan *et al.*, 2011) or high values of NDWI (Delbart *et al.*, 2005).

For long-term VI data record, the noises also result from instrumental uncertainties related to sensor decay and inconsistency among multi-sensors. A variety of studies have simulated VI values across different sensors to investigate the uncertainty caused by various impact factors and to establish VI translation equations. Generally, the VI values from various instruments are continued using a set of linear or quadric equations (Steven *et al.*, 2003; Fensholt and Sandholt, 2005; Miura *et al.*, 2006).

The modeled annual time series of VI data is not necessary for the accurate reflection of seasonal vegetative signals because of the complex abiotic influences. The degree of vegetation representation is strongly dependent on the model approaches used. The uncertainty in the temporal VI trajectory is generally the main source of errors in the detection of vegetation phenologic metrics, which is currently lack of detailed investigations.

A number of methods have been developed to identify the timing of phenological phases (or metrics) from the modeled/smoothed temporal VI trajectory at regional and global scales.

The commonly used methods are the threshold-based technique which is divided into absolute VI threshold (e.g., Lloyd, 1990; Fischer, 1994; Myneni *et al.*, 1997; Zhou *et al.*, 2001) and relative threshold (e.g., White *et al.*, 1997; Jonsson and Eklundh, 2002; Delbart *et al.*, 2005; Karlsen *et al.*, 2006; Dash *et al.*, 2010), moving average (Reed *et al.*, 1994), spectral analysis (Jakubauskas *et al.*, 2001; Moody and Johnson, 2001), and inflection point estimation in the time series of vegetation indices (Moulin *et al.* 1997; Zhang *et al.* 2003; Tan *et al.*, 2011). Various approaches in detecting phenological timing, particularly the greenup onset, are compared using the same dataset (de Beurs and Henebry, 2010; White *et al.*, 2009). Evidently, most of the methods work well at local and regional scales, or for specific vegetation types. However, they are difficult to implement globally since empirical constants are involved and generally do not account for ecosystem specific characteristics of vegetation growth.

3. Long-term satellite detection of global vegetation phenology

3.1 Global vegetation phenological metrics

Phenology observed from satellite data is usually defined as land surface phenology (de Beurs and Henebry, 2004; Friedl et al., 2006) because an annual cycle of satellite data reflects seasonal variation composed of vegetation, atmosphere, snow cover, water conditions, and other land disturbance. However, vegetation seasonal dynamics are generally the parameters of interest to retrieve, whereas the abiotic signals in the temporal satellite data are considered to be noise. As a result, long-term global satellite-based phenological metrics in this chapter are defined according to vegetation seasonal cycles. Briefly, a seasonal cycle of vegetation growth consists of a greenup phase, a maturity phase, a senescent phase, and a dormant phase (Figure 1, Zhang *et al.*, 2003). These four phases are characterized using four phenological transition dates in the time series of VI data: (1) greenup onset (leaf-out): the date of onset of VI increase; (2) maturity onset: the date of onset of VI maximum; (3) senescence onset: the date of onset of VI decrease; and (4) dormancy onset: the date of onset of VI minimum. Furthermore, the time series of VI data provides the integrated VI for the growing season (the sum of daily VI values varying from greenup onset to dormancy onset), maximum and minimum VI values during a growing season, and the length of the vegetation growing season.

During a senescent phase, foliage senescent development consists of several coloration statuses (Zhang and Goldberg, 2011). Fall foliage coloration is a phenomenon occurring in many deciduous trees and shrubs worldwide. Fall foliage status is a function of the colored leaves on the plant canopy. With the spread of colored foliage, the percentage of fallen leaves increases. Their difference represents relative variation in colored leaves on plant canopy, which can be quantified using a temporally-normalized brownness index. The occurrence of the maximum relative variation derived from the brownness index is considered to be a critical point in foliage coloration status, this being the onset timing of peak foliage coloration. Prior to this point, foliage status is generally defined using the categories of little/no change, low coloration, moderate coloration, and near-peak coloration. Following the critical point, it is divided into peak coloration phase and post-peak coloration phase (Figure 2).
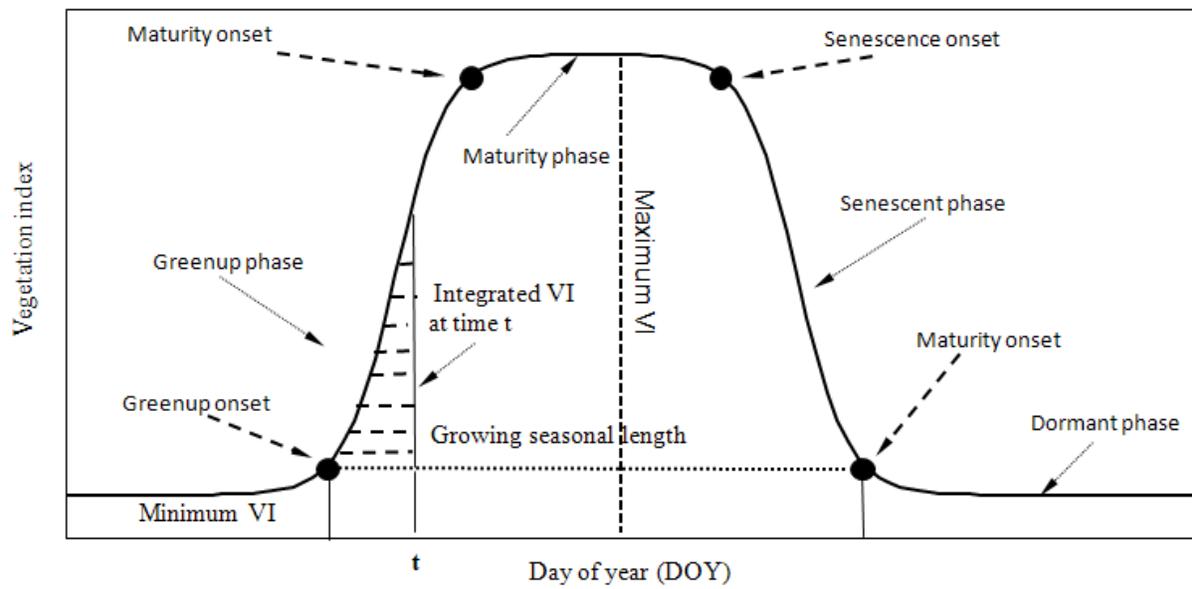
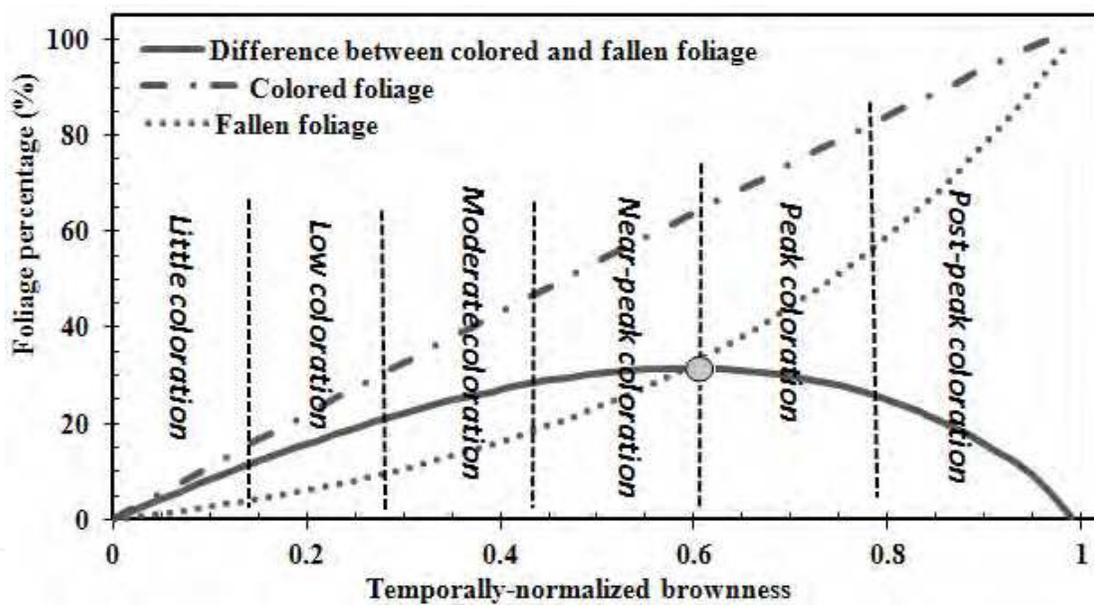Fig. 1. Key phenological metrics in an annual trajectory of satellite vegetation index.

Fig. 2. Correlation of the temporally-normalized brownness index with colored leaves and fallen leaves, separately, and determination of foliage coloration status. The grey dot indicates the critical point when colored foliage reaches maximum on a plant canopy.

More than one set of vegetation phenological metrics could occur within a one-year period because of the complexity of phenological cycles across the globe. Vegetation growth can undergo one or more cycles, and may include an incomplete cycle (truncated at the beginning or end) during a year (Figure 3). The simplest case is illustrated in Figure 3a, where a single and complete growth cycle centers near the mid-point of a 12-month period. Two partial cycles are recorded in Figure 3b, 3c, and 3d. Figure 3e illustrates the situation where two complete growth cycles are finished, which leads to two complete sets of phenological metrics. Figure 3f–3h shows examples of two incomplete cycles and one complete cycle. To capture vegetation phenological timing properly from the complex cycles

within a given one-year period, the satellite data should be extended by periods of a half-year prior to and following the period of interest, separately.
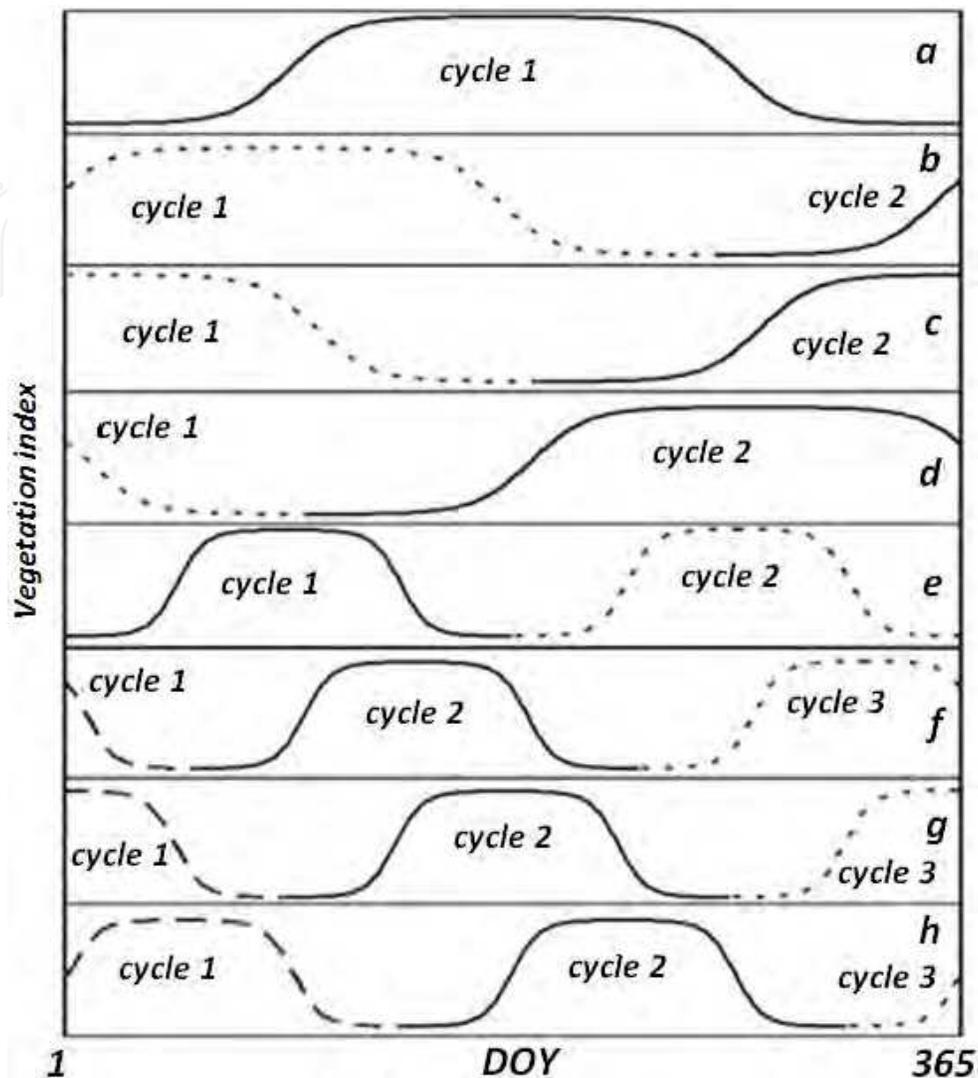

Fig. 3. Various hypotheses of vegetation phenological cycles across the globe.

3.2 Detection of global vegetation phenology

To determine the global phenological metrics described above, the following approaches are conducted. Temporal VI data are first preprocessed to remove or reduce the impacts of clouds, atmosphere, snow cover, etc. Specifically, the data gaps caused by clouds–creating isolated missing values–are filled by linear interpolation using neighbor good quality data. The time series of VI data at each pixel is then smoothed using a Savitzky-Golay and running local median filter. The background VI value at each pixel, which represents the minimum VI of soil and vegetation in an annual time series (Zhang *et al.*, 2007), is identified and it is used to replace VI values in the time series flagged as snow contaminations.

Vegetation growth cycle is identified using a moving slope along the VI time series. The periods with sustained VI increase and decrease at each pixel are determined using a five-point moving slope technique, where transitions from periods of increasing VI to periods of

decreasing VI are identified by changes from positive to negative slope, and vice versa. Because slight decreases or increases in VI can be caused by local or transient processes unrelated to vegetation-growth cycles, two heuristics are applied to exclude such variation: (1) the change in VI within any identified period of VI increase or decrease must be larger than 35% of the annual range in VI for that pixel; and (2) the ratio of the local maximum VI to the annual maximum VI should be at least 0.7. This approach screens out short-term variation unrelated to growth and senescence cycles in VI data, while at the same time identifying multiple growth cycles within any 12-month period.

VI time series in the growing phases (VI consistent increase) and senescent phases (VI consistent decrease) is modeled using a sigmoidal vegetation growth function (Zhang et al., 2003). The specific sigmoid function used to model temporal VI dynamics is the logistic function of vegetation growth:

$$y(t) = \frac{c}{1 + e^{a+bt}} + d \tag{4}$$

where t is time in days, $y(t)$ is the VI value at time t, a and b are free parameters that are fitted using a non-linear least sqaures approach, c is the amplitude of VI variation and d is the initial background VI value. The advantages of the sigmoidal model are that: (1) it provides a simple, bounded, continuous function for modeling growth and decay processes; and that (2) each parameter can be assigned a biophysical meaning related to vegetation growth or senescence.

This sigmoidal model has been demonstrated to be effective in depicting seasonality of vegetation growth as a function of time (or cumulative temperature) in various ecosystems and data measurements. It was originally developed for monitoring crop growth based on field measurements (e.g., Richards, 1959; Ratkowsky, 1983) and adopted to simulate temporal satellite vegetation index (Zhang *et al*., 2003). It has then been applied to investigate seasonal vegetation growth using webcam data (Richardson *et al*., 2006; Kovalskyy *et al*., 2012), Landsat TM data (e.g., Fisher *et al*., 2006; Kovalskyy *et al*., 2011), AVHRR data (e.g., Zhang *et al*., 2007), and MODIS data (e.g., Zhang *et al*., 2003, 2006; Ahl *et al*., 2006; Liang *et al*., 2011). Moreover, studies have shown that the sigmoidal model performance is superior to both Fourier functions and asymmetric Gaussian functions for dictping remotely sensed phenology (Beck *et al*., 2006). Thus, the physically-based sigmoidal model is applicable for the detection of global vegetation phenology.

Phenological transition dates within each growth or senescence phase are identified using the rate of change in the curvature of the modeled sigmoidal curves (Zhang et al., 2003; Figure 1). Specifically, transition dates correspond to the day-of-year (DOY) on which the rate of change in curvature in the VI data exhibits local minima or maxima. These dates indicate when the annual cycle makes a transition from one approximately linear stage to another. Formally, at any time t, the curvature (K) for the sigmoidal function given above is:

$$K = \frac{d\alpha}{ds} = \frac{y''}{\left(1 + y'^2\right)^{\frac{3}{2}}} = -\frac{b^2 c e^{a+bx}\left(1 - e^{a+bx}\right)\left(1 + e^{a+bx}\right)^3}{\left[\left(1 + e^{a+bx}\right)^4 + b^2 c^2 e^{2(a+bx)}\right]^{\frac{3}{2}}} \tag{5}$$

where α is the angle (in radians) of the unit tangent vector at time t along a differential curve, and s is the unit length of the curve. Setting $z = e^{a+bt}$, the rate of change of curvature (K') is:

$$K' = b^3 cz \left\{ \frac{3z(1-z)(1+z)^3 \left[2(1+z)^3 + b^2 c^2 z \right]}{\left[(1+z)^4 + (bcz)^2 \right]^{\frac{5}{2}}} - \frac{z^2 (1 + 2z - 5z^2)}{\left[(1+z)^4 + (bcz)^2 \right]^{\frac{3}{2}}} \right\} \quad (6)$$

During the growth period, when vegetation transitions from a dormant state to a growth phase, three extreme points in a VI curve can be identified using the equation 6 (Zhang *et al.*, 2003). The two maximum values correspond to the onset of greenup (onset of VI increase) and the onset of maturity (onset of VI maximum), respectively (Figure 1). Similarly, the extreme points during the senescent phase represent the transition dates of the senescent onset (onset of VI decrease) and the dormancy onset (onset of VI minimum).

To determine foliage coloration status, a temporally-normalized brownness index is derived from the relative percentage dynamics of the fraction of colored foliage (Zhang and Goldberg, 2011). This brownness index is described as:

$$\text{TNBI}_{b(t)} = \frac{F_{c(t)} - F_c \min}{F_c \max - F_c \min} = \frac{F_{cb(t)} - F_{cb} \min}{F_{cb} \max - F_{cb} \min} \quad (7)$$

where $F_{cbmin} = F_{cmin} + F_b$; $F_{cbmax} = F_{cmax} + F_b$; $F_{cb(t)} = F_{c(t)} + F_b$; $\text{TNBI}_{b(t)}$ is defined as the temporally-normalized brownness at time t; F_b is the exposed surface background; $F_{c(t)}$ and $F_{cb(t)}$ are the fraction of colored foliage on plant canopy and total brown material at time t, separately; F_{cmin} and F_{cmax} are the maximum and minimum fractions of colored leaf cover; and F_{cbmin} and F_{cbmax} are the minimum and maximum fractions of brown material during the senescent phase, separately.

The temporally-normalized brownness index is directly linked to the temporal trajectory of vegetation index (Zhang and Goldberg, 2011). Specifically, the colored foliage is determined after the modeled temporal VI trajectory during the senescent phase is further combined with a linear mixture model of surface components consisting of green (or photosynthetic) vegetation, colored (or non-photosynthetic) vegetation, and exposed surface background (bare soil and rock). As a result, the temporally-normalized brownness index is deduced as:

$$\text{TNBI}_{b(t)} = 1 - \frac{1}{1 + e^{a+bt}} \quad (8)$$

The temporally-normalized brownness index represents relative changes in colored foliage, and varies with time in each pixel individually. It is independent of the surface background, vegetation abundance, and species composition. Thus, it is robust to divide the foliage coloration status, as displayed in Figure 2, into separate categories of little coloration, low coloration, moderate coloration, near-peak coloration, peak coloration, and post-peak coloration.

3.3 Vegetation index for global phenology detection

A long-term dataset of global EVI2 has been generated from the daily land surface reflectance from the AVHRR Long-Term Data Record (LTDR) and the MODIS Climate Modeling Grid (CMG) records. AVHRR LTDR provides daily surface spectral reflectance at a spatial resolution of 0.05 degrees from various AVHRR sensors from 1981–1999 (Vermote and Saleous, 2006), which is available at the NASA funded REASoN project web site (http://ltdr.nascom.nasa.gov/). The MODIS CMG dataset provides Terra and Aqua MODIS daily CMG surface reflectance (Collection 5.0) at a spatial resolution of 0.05 degrees, covering the period from 2000 to 2010, which is available at the USGS for EROS DAAC (http://edcdaac.usgs.gov/main.asp). From these daily surface spectral reflectance, the long-term daily EVI2 has been calculated and available for the last 30 years (http://vip.arizona.edu/viplab_data_explorer).

4. Results in global vegetation greenup onset

Global vegetation phenological metrics during the last three decades were detected from global daily EVI2 using a series of piece-wise logistic models. Here, only the greenup onset is presented and discussed because it is the most important parameter in a vegetation seasonal cycle.

4.1 Spatial pattern in the timing of greenup onset

Figure 4 sets out the average onset of vegetation greenup in the 1980s, 1990s, and 2000s. If there were multiple seasonal cycles in a given calendar year, the first occurrence of greenup onset was selected. As expected, the spatial pattern in the three periods is very similar. However, the spatial variation in phenological transition dates reflects both broad-scale patterns in controlling mechanisms related to climate, and more local factors related to land cover and human activities.

Several spatially distinctive properties of greenup onset are evident. Changes in phenology with latitude are apparent in most of the northern hemisphere, from 30°N northwards (Figure 4). Greenup onset occurs in early March in the southern USA (south of 40°N), April in the northern USA, and at the end of June in northern Canada. Zonal patterns in the timing of greenup onset indicate that the transition date of greenup varies at a rate of about 2–3 days per degree of latitude in North America, Europe, and Asia (Figure 5a, 5b). This latitude dependence is assumed to be a function of temperature variation (Myneni *et al.*, 1997; Zhang *et al.*, 2004a).

The dependence on latitude is spatially variable because of the spatial complexity in elevation and human activities. For example, the timing shift in greenup onset is about one and half months from bottom to top of the Carpathian Mountains and Dinaric Alps in Europe (Figure 5b). This reflects that the timing of greenup onset is also a function of elevation in mountains, because temperature decreases with increasing elevation. Moreover, agricultural land use is one of the most geographically extensive land cover types on the Earth. Their phenological behavior is frequently distinct from that of surrounding natural vegetation because of controls applied by human management. It is highly evident in central North America, where the onset of greenup occurs much later in the Mississippi River

valley and the mid-western agricultural heartland, relative to the surrounding natural vegetation (Figure 4). This pattern depends strongly on crop type and human management. Moreover, urban lands advance greenup onset relative to rural areas surrounding the urban regions because of the urban heat island effects (Zhang *et al.*, 2004b), although this is not clearly visualized on the 0.05 degree maps.

In dry climate (arid and semi-arid regions), the spatial pattern in vegetation greenup onset is very complex because it is generally controlled by water availability. In Mediterranean climates and the southwestern United States, the start of vegetation growth occurs mainly in winter and early spring and, in some cases, during the summer monsoon season. Outside of the humid tropical regime in sub-Saharan Africa, Australia, and southern South America, the dominant vegetation types are grasses, shrubs and savannas. The onset of vegetation greenup in these vegetation types generally depends on timing of the rainy season.

Inspection of the greenup onset in dry climates reveals several regular patterns in local regions. The most notable pattern is present in northern Africa (the Sahelian and sub-Sahelian region). The timing of greenup onset shifts smoothly from early March, at around 6.5°N, to mid-October in the boundary between the Sahel and the Sahara desert (17.9°N, Figure 5b). The shift rate is about 20 days per degree of latitude, which is about 10 times slower than that in temperate North America and Eurasia. This pattern reflects the start of the rainy season, which triggers the onset of vegetation growth in this region (Zhang *et al.*, 2005), which is in turn controlled by the migration of the Intertropical Convergence Zone (ITCZ). In contrast, the phenological pattern found in southern Africa is much more complex (roughly 1°S southward), although greenup onset shows a regular delayed shift from 1°S to 22°S and an advanced shift of 22°S southwards (Figures 4 and 5b). In the eastern part of this region, vegetation growth generally starts between September and November, whereas it tends to occur in February and March in southwestern Africa (west of the Kalahari Desert). In the Great Horn of Africa, two cycles of vegetation growth are evident, which reflects the bimodal precipitation regime in this region. These irregular patterns coincide strongly with patterns evident in the arrival of the rainy season (Zhang *et al.*, 2005).

In South America, four different phenological regions follow the variation in the onset of vegetation greenup. Greenup onset occurs in the boreal winter, with no obvious gradient in the northern Andes mountainous region. In southern South America, green leaves emerge in the boreal summer and gradually push northward at a rate of about three days per latitude (Figure 5c). However, a remarkable phenological trend exists along the Brazilian Highlands (in the direction from 60°W and 39°S to 35°W and 5°S), where the greenup onset shifts from July to next February at a rate of about 0.12 days/km. In contrast, the timing of greenup onset is very irregular in the Amazon rainforest, where the values are of poor quality because of high frequencies of cloud cover and weak seasonality in vegetation index. Overall, the complex phenological pattern is likely to be associated with precipitation and latitude-elevation-dependent temperature.

Phenological variation in Australia divides into three distinct regions. Greenup onset occurs in the late boreal autumn and winter in northern areas, in the boreal summer in southern areas, and in the boreal spring, or with no clear phenology, in central Australia. Although
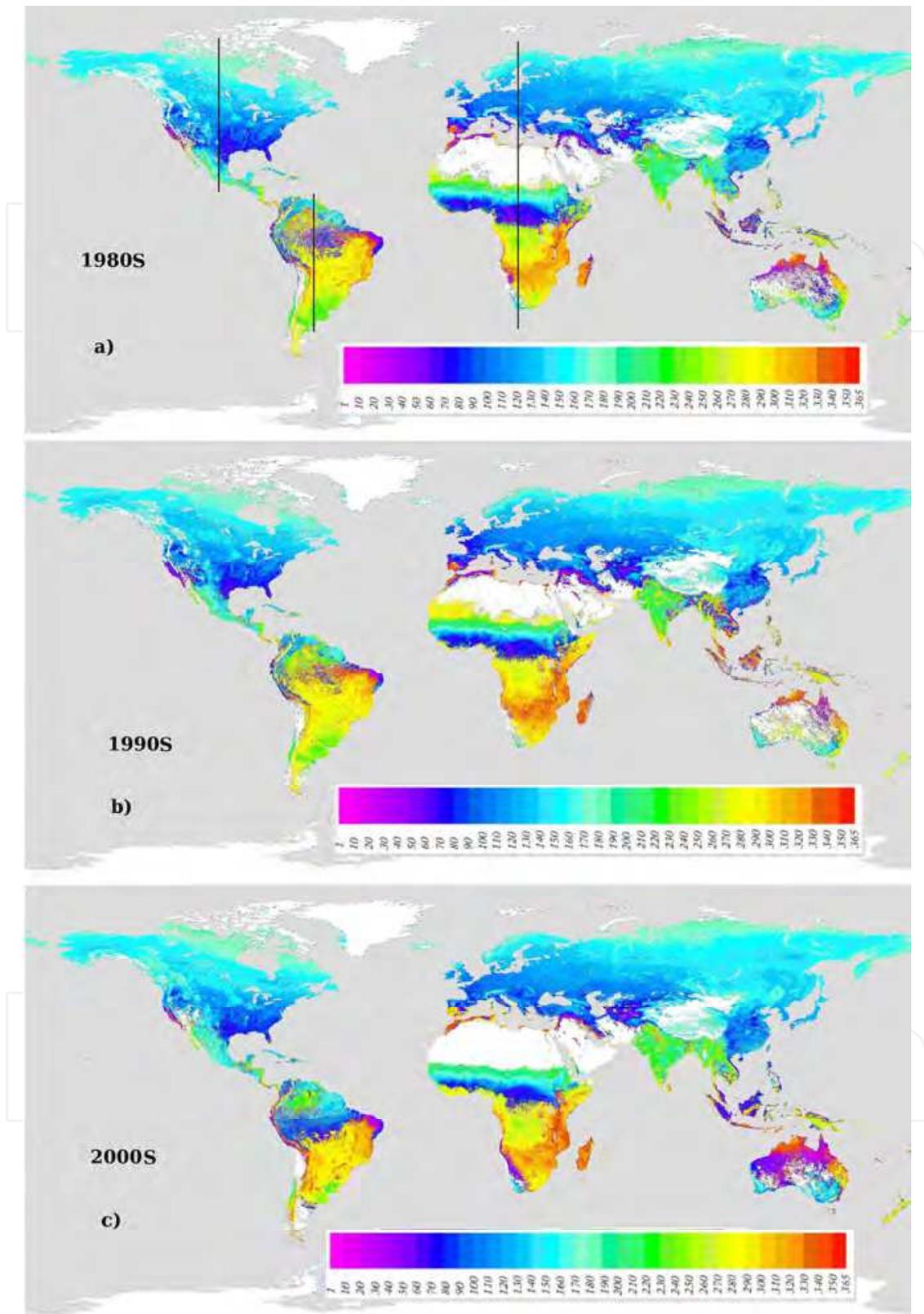
Fig. 4. Average timing of greenup onset in three periods: a) 1980s (1982--1989), b) 1990s (1990--1999), and c) 2000s (2001--2009), separately. The color legend is the day of year. Three vertical lines on a) present the locations of profiles in Figure 5.

irregular patches are observed in each region, a regular gradient is apparent locally. Specifically, the onset of greenup occurs mainly in January over northern Australia, while phenological phases occur about six months later in southern Australia. For example, the timing of greenup onset in central north Australia (13–21.5°S and 128–140°E) shifts at a rate of 0.1 days/km from October to late January. This trend is controlled by the Australian summer monsoon and extra-monsoonal rainfall events (e.g., Hendon and Lebmann, 1990), and also reflects the changes in species composition and a decrease in both tree biomass and diversity (Cook and Heerdegen, 2001).
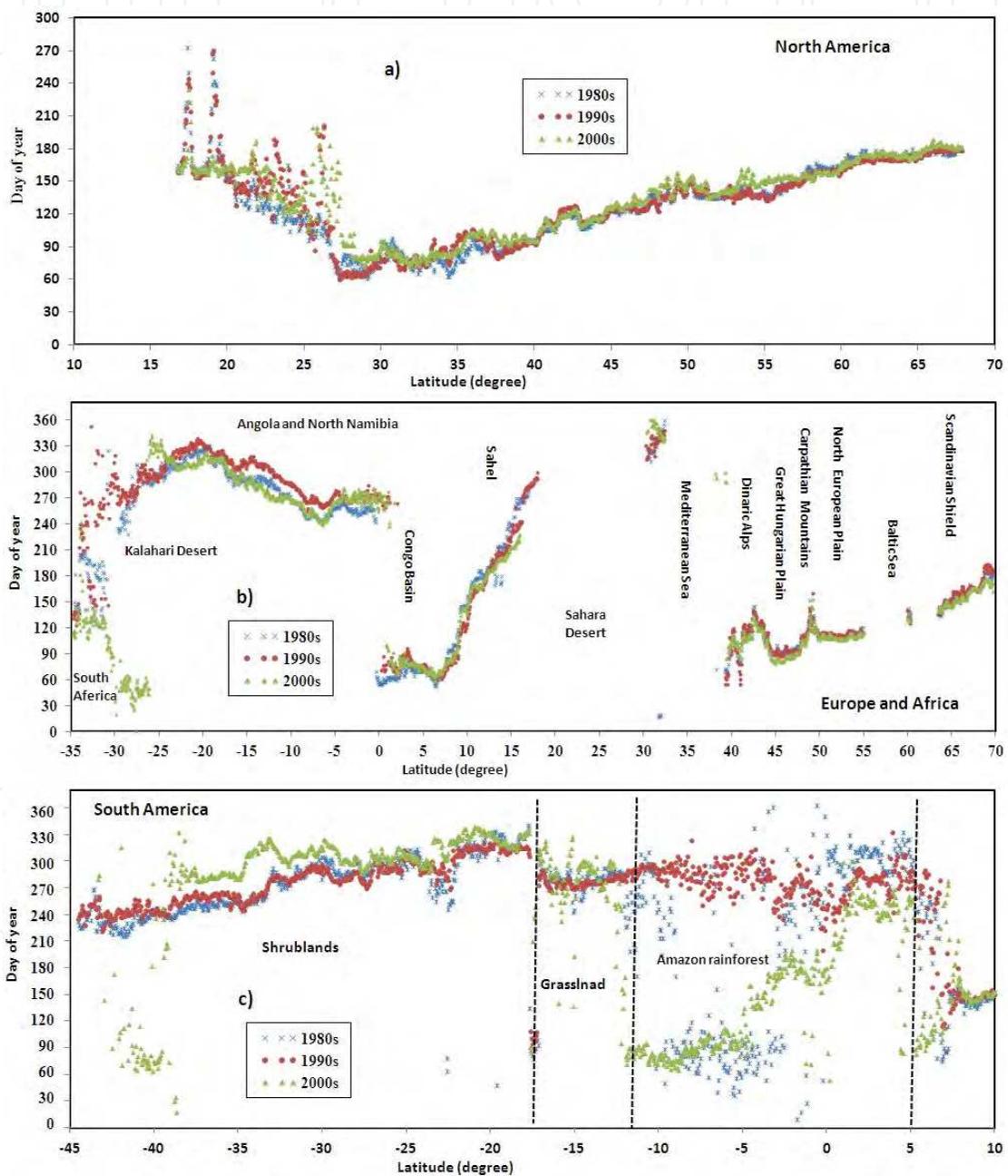
Fig. 5. Profiles of the shift of greenup onset: a) along a meridian of 100°W in North America, b) along a meridian of 20°E in Europe and Africa, and c) along a meridian of 65°W in South America. The geographic locations are displayed on Figure 4a.
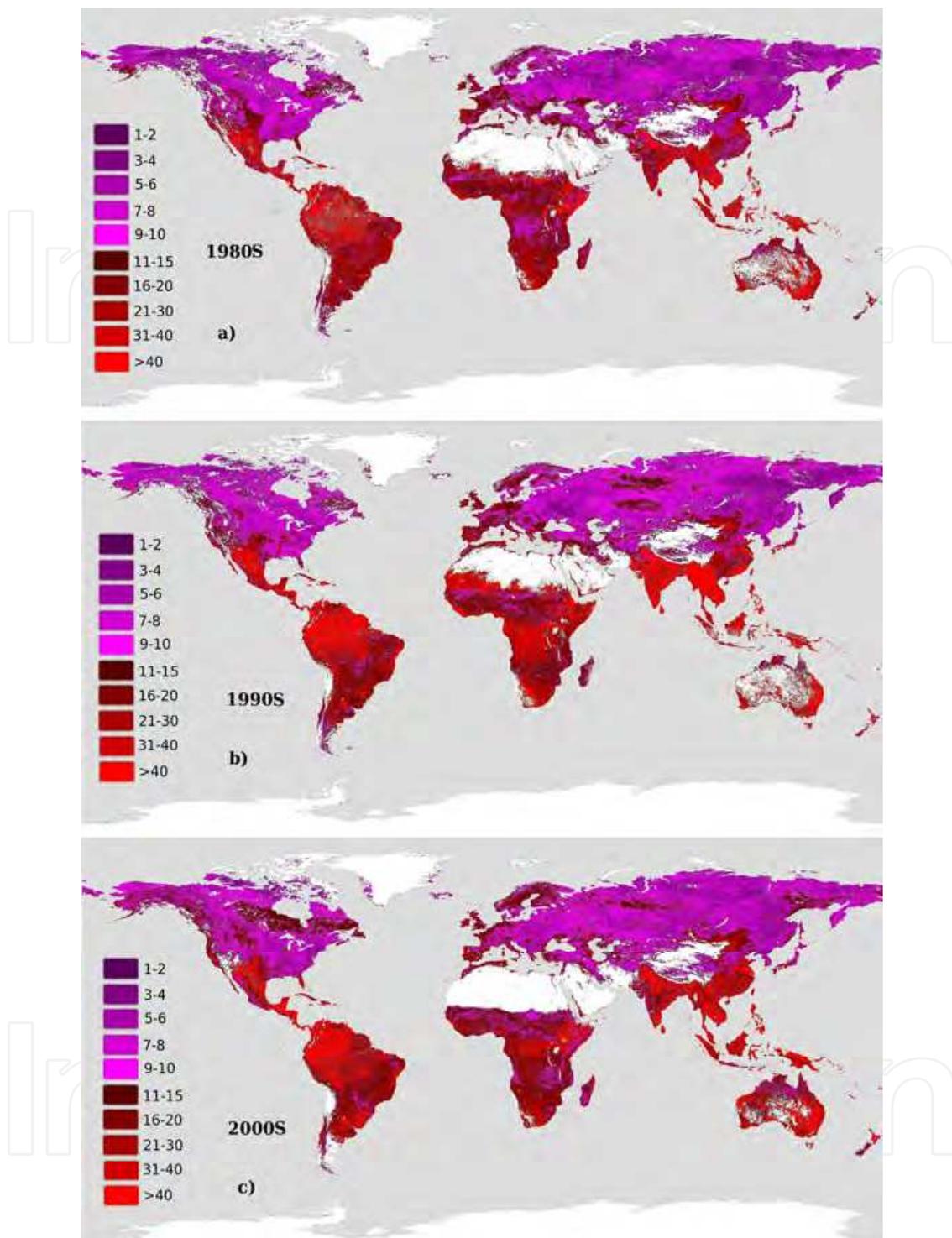
Fig. 6. Inter-annual variation (standard variation) in the timing of greenup onset in a) 1980s, b) 1990s, and c) 2000s, separately. The color legend is the number of days.

Note that the detected phenology metrics are of poor quality for evergreen vegetation (tropical rainforests and boreal forests) in many areas. This is because the annual variation in EVI2 is too subtle to retrieve phenology effectively. Moreover, there is no vegetation growth in tropical desert areas and polar regions of permanent snow cover.

4.2 Inter-annual variation in greenup onset

Inter-annual variation in greenup onset is limited in temperate and cold climate regimes (Figure 6). In the northern hemisphere, the standard deviation is generally less than 10 days, although there are several locations with a standard deviation of about 11–15 days in evergreen needle leaf forest where EVI2 seasonality is weak. This suggests that spring occurrences of greenup onset are regularly triggered by an increase in spring temperature, which leads to a comparable annual EVI2 trajectory (Figure 7a).

In contrast, the inter-annual timing of greenup onset varies considerably in arid and semiarid climate regimes (Figure 6). The standard deviation is generally larger than 15 days within each decade. This is probably associated with the fact that vegetation greenup onset strongly tracks rainy season occurrence, which can change greatly between years (Zhang *et al.*, 2005). For example, a temporal EVI2 trajectory in shrubland in the southwestern United States clearly indicates the variability of inter-annual vegetation growing cycles (Figure 7b), with the timing of greenup onset varying from DOY 85 to 213 during the period from 2001 to 2009.
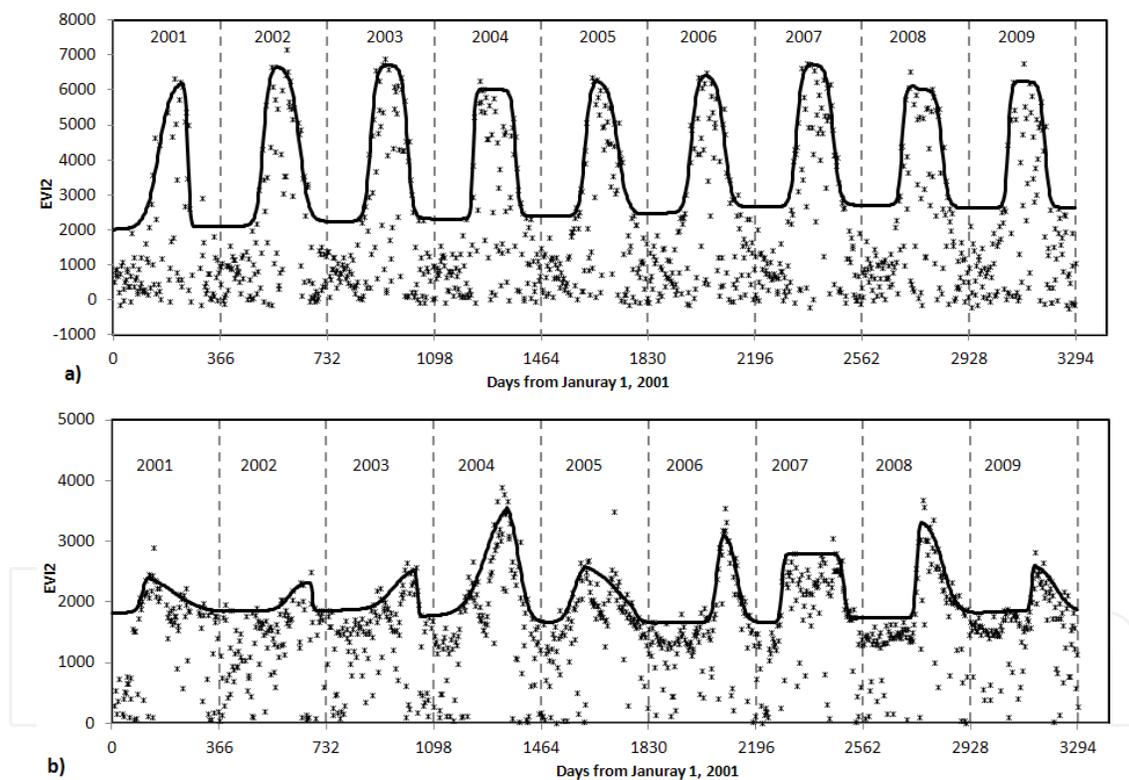

Fig. 7. Time series of daily EVI2 from 2001–2009 in two sample pixels. Solid line is the modeled vegetative EVI2 while the asterisks are the raw EVI2. a) Deciduous forests in northeastern North America and b) shrubland in the semiarid region of southwestern North America.

4.3 Shift in greenup onset

Figure 8 sets out the shift of greenup onset during the past three decades. From the 1980s to the 1990s, the onset of vegetation greenup became advanced in most of the northern

hemisphere, South America, and the Sahelian and sub-Sahelian regions. However, delayed shifts appeared in relatively small regions in each continent, except for the southern semiarid region in Africa.

From the 1990s to the 2000s, shifts in greenup onset were basically opposite to those in the previous period in large parts of South America, Africa, and North America. In contrast, persistent trends during the three decades occurred in relatively small regions. In particular, an advanced trend was evident in most of Eurasia.

It is worth noting that the vegetation greenup occurred in a much larger area across the Sahel in the 1990s than in the 1980s. This trend agrees with the result derived by Tucker and Nicholson (1999) and Olsson *et al.* (2005). However, the region with greenup occurrence was reduced during 2000s, which is probably associated with retreat of the ITCZ migration.
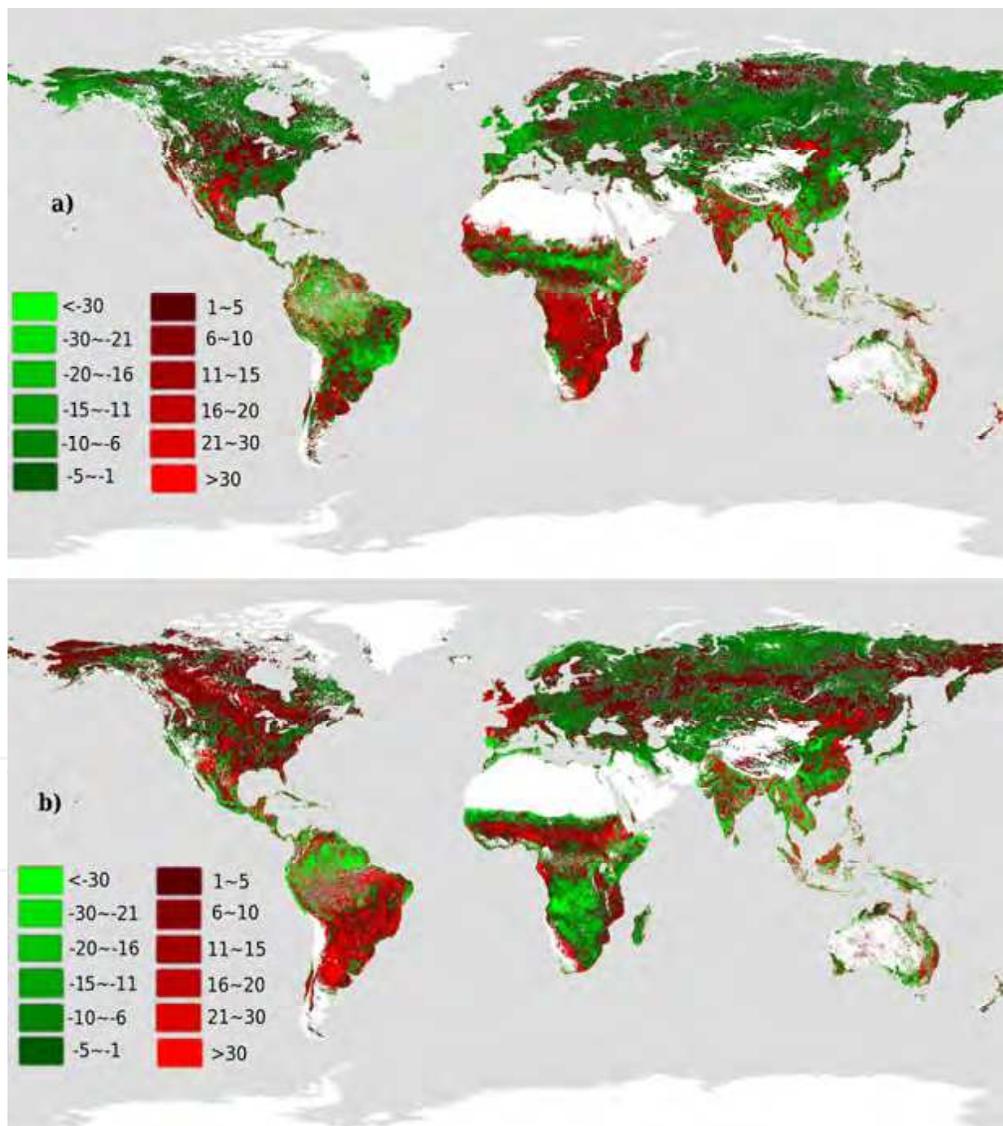

Fig. 8. Shift in greenup onset. a) The difference between the 1990s and 1980s; b) the difference between the 2000s and 1990s. The green color indicates the number of advanced days, while the red color shows delayed days.

5. Discussion and conclusions

This chapter provides an overview of methods and results in the detection of vegetation phenology using satellite data. Various vegetation indices derived from satellite data reflect seasonal dynamics in vegetation growth with reasonable accuracy, and a variety of methods have been developed for detecting vegetation phenological metrics. In the detection of long-term global vegetation phenology, EVI2 from AVHRR and MODIS data has advantages over NDVI and EVI (Rocha and Shaver, 2009) and a series of pieces-wise sigmoidal models of vegetation growth provide a flexible, repeatable, and realistic means to monitor seasonal and inter-annual dynamics in vegetation using remote sensing data across the globe.

At global scales, vegetation greenup onset during the past three decades suggests that AVHRR and MODIS-derived estimates are geographically and ecologically realistic. In particular, patterns in the timing of greenup onset are strongly dependent on latitude (temperature patterns) in temperate and cold climate regimes across the northern hemisphere, although these patterns are also impacted by elevation and human activities locally. Their inter-annual variance is relatively small, with a value generally less than 10 days within each decade. In contrast, greenup onset in arid and semiarid climate regions is very complex. The regular spatial gradient only occurs in local regions, such as the Sahelian and sub-Sahelian region. The inter-annual variance of phenological timing could be larger than one month. This is probably in response to precipitation regimes and rainfall seasonality migrations (Zhang *et al.*, 2005).

The long-term shifts of vegetation phenology in most parts of the globe are generally episodic rather than persistent in response to climate changes. Early trends of greenup onset from the 1980s to the 1990s appear across most of the northern hemisphere, which agrees with previous findings (Zhou *et al.*, 2001; Myneni *et al.*, 1997; Zhang *et al.*, 2007). The consistent advanced trends from the 1980s–1990s–2000s only occur in large parts of Eurasia and small parts of North America. In most regions of South America, the timing of greenup onset shifted from an early trend to a late trend while an opposite shift occurred in Africa. The detailed mechanisms driving these complex trends will be further investigated.

Finally, it is critical to provide the quality and accuracy of satellite global vegetation phenology detections. Without this, trends derived to predict the response to climate change are less reliable. The quality of phenological detection is strongly dependent on the temporal VI trajectory, which is generally affected by the frequency of cloud cover and snow appearance, and by the model efficiency in removing abiotic noise. To validate accuracy, sufficient field measurements comparable to a satellite footprint are required. This requires field data to reconcile with satellite-based phenological observations, which is currently extremely challenging. The validation effort will become more practical, with the inclusion of observations from webcam (Richardson *et al.*, 2009) and the landscape measurements upscaled from field observations (Liang *et al.*, 2011). Currently, the effort to assess the quality and accuracy of global vegetation phenology is underway.

6. Acknowledgements

term EVI2 data. The views, opinions, and findings contained in this study are those of the author(s) and should not be interpreted as an official NOAA or US Government position, policy, or decision.

7. References

Adamsen, F.J., Coffelt, T.A., and Nelson, J.M., Barnes, E.M., and Rice, R.C., 2000. Method for using image from a color digital camera to estimate flower number. *Crop Science*, 44: 704–09.

Ahl, D. E., Gower, S. T., Burrows, S. N., Shabanov, N. V., Myneni, R. B., and Knyazikhin, Y., 2006. Monitoring spring canopy phenology of a deciduous broadleaf forest using MODIS. *Remote Sensing of Environment*, 104(1): 88-95.

Bausch, W. C., 1993. Soil background effects on reflectance-based crop coefficients for corn. *Remote Sensing of Environment*, 46: 213−222.

Beck, P.S.A., Atzberger, C., Høgda, K.A., Johansen, B., and Skidmore, A.K., 2006. Improved monitoring of vegetation dynamics at very high latitudes: A new method using MODIS NDVI. *Remote Sensing of Environment,* 100: 321 – 334.

Ben-Ze'ev, E., Karnieli, A., Agam, N., Kaufman, Y., and Holben, B., 2006. Assessing vegetation condition in the presence of biomass burning smoke by applying the aerosol-free vegetation index (AFRI) on MODIS. *International Journal of Remote Sensing*, 27: 3203−3221.

Bradley, B. A., Jacob, R. W., Hermance, J. F., and Mustard, J. F., 2007. A curve fitting procedure to derive inter-annual phenologies from time series of noisy satellite NDVI data. *Remote Sensing of Environment*, 106: 137–145.

Chen, J., Jonsson, P., Tamura, M., Gu, Z.H., Matsushita, B., and Eklundh, L., 2004. A simple method for reconstructing a high-quality NDVI time-series data set based on the Savitzky-Golay filter. *Remote Sensing of Environment, 91*: 332-344.

Chen, X., Hu, B., and Yu, R., 2005. Spatial and temporal variation of phenological growing season and climate change impacts in temperate eastern China. *Global Change Biology*, 11: 1118–1130.

Cook, G. D., and Heerdegen, R. G., 2001. Spatial variation in the duration of the rainy season in monsoonal Australia. *International Journal of Climatology, 21*: 1723-1732.

Dash, J., Jeganathan, C., and Atkinson, P.M., 2010. The use of MERIS Terrestrial Chlorophyll Index to study spatio-temporal variation in vegetation phenology over India. *Remote Sensing of Environment, 114*: 1388-1402.

de Beurs, K.M., and Henebry, G.M. 2010. Spatio-temporal statistical methods for modeling land surface phenology. In *Phenological Research - Methods for Environmental and Climate Change Analysis*, Irene L. Hudson and Marie R. Keatley (Eds), Spring, New York, pp. 177-208.

de Beurs, K.M., and Henebry, G.M., 2004. Land surface phenology, climatic variation, and institutional change: Analyzing agricultural land cover change in Kazakhstan. *Remote Sensing of Environment, 89*: 497-509.

Delbart, N., Kergoat, L., Le Toan, T., Lhermitte, J., and Picard, G., 2005. Determination of phenological dates in boreal regions using normalized difference water index. *Remote Sensing of Environment, 97*: 26-38.

Fensholt, R. and Sandholt, I., 2005. Evaluation of MODIS and NOAA AVHRR vegetation indices with in situ measurements in a semi-arid environment. *International Journal f Remote Sensing, 26*(12): 2561-2594.

Fisher, A., 1994. A model for the seasonal variations of vegetation indices in coarse resolution data and its inversion to extract crop parameters. *Remote Sensing of Environment*, 48: 220-230.

Fisher, J.I., Mustard, J.F., and Vadeboncoeur, M.A., 2006. Green leaf phenology at Landsat resolution: scaling from the field to the satellite. *Remote Sensing of Environment*, 100: 265–279.

Fitter, A.H., Filtter, R.S.R., Harris, I.T.B., and Williamson, M.H., 1995. Relationship between first flowering date and temperature in the flora of a locality in central England. *Functional Ecology*, 9: 55-60.

Friedl, M.A, Henebry, G., Reed, B. Huete, A., White, M., Morisette, J., Nemani, R., Zhang, X., and Myneni, R., 2006. Land surface phenology: a community white paper requested by NASA. ftp://ftp.iluci.org/Land_ESDR/Phenology_Friedl_whitepaper.pdf.

Friedl, M. A., McIver, D. K., Hodges, J. C. F., Zhang, X. Y., Muchoney, D.,Strahler, A. H., Woodcock, C. E., Gopal, S., Schneider, A., Cooper, A., Baccini, A., Gao, F., and Schaaf, C., 2002. Global land cover mapping from MODIS: algorithms and early results. *Remote Sensing of Environment*, 83: 287-302.

Ganguly, S., Friedl, M.A., Tan, B., Zhang, X., and Verma, M., 2010. Land Surface Phenology from MODIS: Characterization of the Collection 5 Global Land Cover Dynamics Product. *Remote Sensing of Environemt*, 114 (8): 1805-1816, doi:10.1016/j.rse.2010.04.005.

Gitelson, A. A., 2004. Wide dynamic range vegetation index for remote quantification of biophysical characteristics of vegetation. *Journal of Plant Physiology*, 161, 165−173.

Goddijn, L.M. and White, M. 2006. Using a digital camera for water quality measurements in Galway Bay. *Estuar Coast Shelf S,* 66: 429–36.

Hargrove, W.W., Spruce, J.P., Gasser, G.E., and Hoffman, F.M., 2009. Toward a National Early Warning System for Forest Disturbances Using Remotely Sensed Canopy Phenology. *Photogrammetric Engineering and Remote Sensing, 75*: 1150-1156.

Hendon, H. H. and Lebmann, B., 1990. A composite study of the Australian summer monsoon. *Journal of Atmospheric Science*, 47: 2227-2240.

Holben, B.N., 1986. Characteristics of maximum value composite images from temporal AVHRR data. *International Journal of Remote Sensing, 7*: 1417-1434.

Huete, A. R., Didan, K., Miura, T., Rodriguez, E. P., Gao, X., and Ferreira, L. G., 2002. Overview of the radiometric and biophysical performance of the MODIS vegetation indices. *Remote Sensing of Environment*, 83: 195−213.

Huete, A. R., Didan, K., Shimabukuro, Y. E., Ratana, P., Saleska, C. R., Hutyra, L. R., Yang, W., Nemani, R.R., and Myneni, R., 2006. Amazon rainforests green-up with sunlight in dry season. *Geophysical Research Letters*, 33, L06405. doi:10.1029/2005GL025583.

Huete, A. R., Jackson, R. D., and Post, D. F., 1985. Spectral response of a plant canopy with different soil backgrounds. *Remote Sensing of Environment*, 17: 37−53.

IPCC 2007 *Climate Change 2007: Impacts, Adaptation, and Vulnerability.* Contribution of Working Group II to the Fourth Assessment Report of the Intergovernment Panel on Climate Change, ed M L Parry, O F Canziani, J P Palutikof, P J van der Linden and C E Hanson (Cambridge: Cambridge University Press) 976pp.

Jakubauskas, M.E., Legates, D.R., and Kastens, J.H., 2001. Harmonic analysis of time-series AVHRR NDVI data. *Photogrammetric Engineering and Remote Sensing, 67*: 461-470.

Jiang, Z., Huete, A.R., Didan, K., and Miura, T., 2008. Development of a two-band enhanced vegetation index without a blue band. *Remote Sensing of Environment*, 112: 3833–3845.

Jönsson, P., Eklundh, L., 2002. Seasonality extraction by function fitting to time-series of satellite sensor data. *IEEE Geosciences and Remote Sensing*, 40: 1824–1831.

Karlsen, S.R., Elvebakk, A., and Hogda, K.A. et al., 2006. Satellite-based mapping of the growing season and bioclimatic zones in Fennoscandia. *Global Ecology Biogeography*, 15: 416–430.

Kaufman, Y. J., and Tanré, D., 1992. Atmospherically resistant vegetation index (ARVI) for EOS-MODIS. *IEEE Transactions on Geoscience and Remote Sensing*, 30: 261−270.

Kovalskyy, V., David, P. Roy, D.P., Zhang, X., and Ju, J., 2012. The suitability of multi-temporal web-enabled Landsat data NDVI for phenological monitoring – a comparison with flux tower and MODIS NDVI. *Remote Sensing Letters*, 3(4): 325–334.

Kramer, K., 1996. *Phenology and growth of European trees in relation to climate change*. Thesis Landbouw Universiteit Wageningen.

Kramer, K., Leinonen, I., and Loustau, D., 2000. The importance of phenology for the evaluation of impact of climate change on growth of boreal, temperate and Mediterranean forests ecosystems: An overview. *International Journal of Biometeorology*, 44: 67-75.

Lauscher, F, 1978. Neue Analysen ältester und neuerer phänologischer Reihen. *Arch. für Meteorologie, Geophysik und Klimatologie (Ser. B)*, 26: 373-385.

Liang, L., Schwartz, M. D., and Fei, S., 2011. Validating satellite phenology through intensive ground observation and landscape scaling in a mixed seasonal forest. *Remote Sensing of Environment*, 115: 143-157.

Lloyd, D., 1990. A phenological classification of terrestrial vegetation cover using shortwave vegetation index imagery. *International Journal of Remote Sens*ing, 11: 2269-2279.

Loveland, T. R., Zhu, Z. L., Ohlen, D. O., Brown, J. F., Reed, B. C., and Yang, L. M., 1999. An analysis of the IGBP global land-cover characterization process. *Photogrammetric Engineering and Remote Sensing*, 65: 1021-1032.

Miura, T., Huete, A. R., and van Leeuwen, W. J. D., 1998. Vegetation detection through smoke-filled AVHRIS images: An assessment using MODIS band passes. *Journal of Geophysical Research*, 103(D24): 32, 001−32,011.

Miura, T., Huete, A., and Yoshioka, H., 2006. An empirical investigation of cross-sensor relationships of NDVI and red/near-infrared reflectance using EO-1 hyperion data. *Remote Sensing of Environment*, 100 (2): 223-236.

Moody, A., and Johnson, D.M., 2001. Land-surface phenologies from AVHRR using the discrete Fourier transform. *Remote Sensing of Environment*, 75: 305–323.

Morisette, J.T., Richardson, A.D., Knapp, A.K., Fisher, J.I., Graham, E.A., Abatzoglou, J., Wilson, B.E., Breshears, D.D., Henebry, G.M., Hanes, J.M., and Liang, L., 2009. Tracking the rhythm of the seasons in the face of global change: phonological research in the 21st century. *Front Ecology Environment*, 7: 253-260, doi:10.1890/070217

Moulin, S., Kergoat, L., Viovy, N., and Dedieu, G.G., 1997. Global-scale assessment of vegetation phenology using NOAA/AVHRR satellite measurements. *Journal of Climate*, 10: 1154-1170.

Myneni, R. B., Keeling, C. D., Tucker, C. J., Asrar, G., and Nemani, R. R., 1997. Increased plant growth in the northern high latitudes from 1981– 1991. *Nature,* 386: 698–702.

Myneni, R.B., S. Hoffman, Y. Knyazikhin, J. L. Privette, J. Glassy, Y. Tian, Y. Wang, X. Song, Y. Zhang, G. R. Smith, A. Lotsch, M. Friedl, J. T. Morisette, P. Votava, R. R. Nemani and S. W. Running, 2002. Global products of vegetation leaf area and fraction absorbed PAR from year one of MODIS data. *Remote Sensing of Environment*, 83: 214-231.

Nemani, R.R., Keeling, C.D., Hashimoto, H., Jolly, W.M., Piper, S.C., Tucker, C.J., Myneni, R.B., and Running, S.W., 2003. Climate-driven increases in global terrestrial net primary production from 1982 to 1999. *Science*, 300(5625):1560-1563.

Olsson, L., Eklundh, L., and Ardö, J., 2005. Greening of the Sahel – trends, patterns and hypotheses. *Journal of Arid Environments*, 63: 556-566.

Parmesan, C., and Yohe, G., 2003. A globally coherent fingerprint of climate change impacts across natural systems. *Nature*, 421: 37-42.

Ratkowsky, D. A., 1983. *Nonlinear regression modeling – A unified practical approach*. New York: Marcel Dekker. (pp. 61– 91).

Reed, B. C., Brown, J. F., VanderZee, D., Loveland, T. R., Merchant, J. W., and Ohlen, D. O., 1994. Measuring phenological variablity from satellite imagery. *Journal of Vegetation Science*, 5: 703-714.

Richards, F.J., 1959. A flexible growth function for empirical use. *Journal of Experimental Botany*, 10, 290-300.

Richardson, A. D., Braswell, B. H., Hollinger, D., Jenkins, J. P., and Ollinger, S. V., 2009. Near-surface remote sensing of spatial and temporal variation in canopy phenology. *Ecological Applications*, 19(6): 1417−1428.

Richardson, A.D., Bailey, A.S., Denny, E.G., Martin, C.W., and O'Keefe, J., 2006. Phenology of a northern hardwood forest canopy. *Global Change Biology*, 12: 1174–1188.

Richardson, A.D., Jenkins, J. P., and Braswell, B.H., *et al.* 2007. Use of digital webcam images to track spring green-up in a deciduous broadleaf forest. *Oecologia,* 115522: 323–34.

Rocha, A.V., Potts, D.L., Goulden, M.L., 2008. Standing litter as a driver of interannual CO_2 exchange variability in a freshwater marsh. *Journal of Geophysical Research*, 113, G04020, doi:10.1029/2008JG000713.

Rocha, A.V., and Shaver, G.R., 2009. Advantages of a two band EVI calculated from solar and photosynthetically active radiation fluxes. *Agricultural and Forest Meteorology*, 149(9): 1560-1563.

Rötzer, T., and Chmielewski, F.M., 2000. Phenological maps of Europe. *Agrarmeteorologische Schriften*, *H6*, 1-12.

Rouse, J.W., Haas, R.H., Schell, J.A., and Deering, D.W., 1973. Monitoring vegetation systems in the Great Plains with ERTS. In *3rd ERTS Symposium, NASA* SP-351 I, pp. 309–317.

Smith, M. O., Ustin, S. L., Adams, J. B., and Gillespie, A. R., 1990. Vegetation in deserts: I. A regional measure of abundance from multispectral images. *Remote Sensing of Environment*, 31: 1-26.

Sparks, T.H., and Carey, P.D., 1995. The responses of species to climate over 2 centuries-an analysis of the Marsham phonological record, 1736-1947. *Journal of Ecology*, 83: 321-329.

Steven, D. M., Malthus, J. T., Baret, F., Xu, H., and Chopping, J. M., 2003. Intercalibration of vegetation indices from different sensor systems. *Remote Sensing of Environment*, 88: 412−422.

Tan, B., J.T. Morisette, R.E. Wolfe, F. Gao, G.A. Ederer, J. Nightingale, and J.A. Pedelty. 2011. An enhanced TIMESAT algorithm for estimating vegetation phenology metrics from MODIS data. *IEEE Journal of Selected Topics in Applied Earth Observations and Remote Sensing*, 4(2): 361-371.

Tucker, C.J., and Nicholson, S.E., 1999. Variations in the size of the Sahara desert from 1980 to 1997, *Ambio*, 28(7): 587-591.

Tucker, C.J., Fung, I.Y., Keeling, C.D., and Gammon, R.H., 1986. Relationship between atmosphere CO2 variations and a satellite-derived vegetation index. *Nature*, 319:195-199.

Unganai, L. S., and Kogan, F. N. 1998. Drought monitoring and corn yield estimation in Southern Africa from AVHRR data. *Remote Sensing of Environment*, 63: 219−232.

Vermote, E.F., and Saleous, N., 2006. Calibration of NOAA16 AVHRR over a desert site using MODIS data. *Remote Sensing of Environment*, 105: 214-220.

Verstraete, M.M., Gobron, N., Aussedat, O., Robustelli, M., Pinty, B., Widlowski, J.L., and Taberner, M., 2008. An automatic procedure to identify key vegetation phenology events using the JRC-FAPAR products. *Advances in Space Research*, 41(11): 1773-1783.

Viovy, N., Arino, O., and Belward, A.S., 1992. The Best Index Slope Extraction (Bise) - a Method for Reducing Noise in Ndvi Time-Series. *International Journal of Remote Sensing,* 13: 1585-1590.

White, M. A., Thornton, P. E., and Running, S. W., 1997. A continental phenology model for monitoring vegetation responses to interannual climatic variability. *Global Biogeochemical Cycles*, 11: 217– 234.

White, M.A., de Beurs, K.M., Didan, K., Inouye, D.W., Richardson, A.D., Jensen, O.P., O'Keefe, J., Zhang, G., Nemani, R.R., van Leeuwen, W.J.D., Brown, J.F., de Wit, A., Schaepman, M., Lin, X.M., Dettinger, M., Bailey, A.S., Kimball, J., Schwartz, M.D., Baldocchi, D.D., Lee, J.T., and Lauenroth, W.K., 2009. Intercomparison, interpretation, and assessment of spring phenology in North America estimated from remote sensing for 1982-2006. *Global Change Biology,* 15: 2335-2359.

White, M.A., Running, S.W., and Thornton, P.E., 1999. The impact of growing-season length variability on carbon assimilation and evapotranspiration over 88 years in the eastern US deciduous forest. *International Journal of Biometeorology*, 42: 139-145.

Zhang, X. and Goldberg, M, 2011. Monitoring Fall Foliage Coloration Dynamics Using Time-Series Satellite Data. *Remote Sensing of Environment,* 115(2): 382-391.

Zhang, X., Friedl, M. A., Schaaf, C. B., and Strahler, A. H., 2004a. Climate controls on vegetation phenological patterns in northern mid- and high latitudes inferred from MODIS data. *Global Change Biology*, 10: 1133–1145.

Zhang, X., Friedl, M. A., Schaaf, C. B., Strahler, A.H., Hodges, J. C. F., Gao, F., Reed, B. C., and Huete, A., 2003. Monitoring vegetation phenology using MODIS. *Remote Sensing of Environment*, 84, 471-475.

Zhang, X., Friedl, M.A., and Schaaf, C.B., 2006. Global vegetation phenology from MODIS: Evaluation of global patterns and comparison with in situ measurements. *Journal of Geophysical Research,* 111, G04017, doi:10.1029/2006JG000217.

Zhang, X., Friedl, M.A., Schaaf, C. B., Strahler, A.H., and Schneider, A., 2004b. The footprint of urban climates on vegetation phenology. *Geophysical Research Letter*, 31, L12209, doi:10.1029/2004GL020137.

Zhang, X., Friedl, M.A., Schaaf, C.B., Strahler, A.H., and Liu, Z., 2005. Monitoring the response of vegetation phenology to precipitation in Africa by coupling MODIS and TRMM instruments. *Journal of Geophysical Research-Atmospheres*, 110:D12103, doi:10.1029/2004JD005263.

Zhang, X., Tarpley, D., and Sullivan, J., 2007. Diverse responses of vegetation phenology to a warming climate, *Geophysical Research Letters*, 34: L19405, doi:10.1029/2007GL031447.

Zhou, L., Tucker, C.J., Kaufmann, R.K., Slayback, D., Shabanov, N.V., and Myneni, R.B., 2001. Variation in northern vegetation activity inferred from satellite data of vegetation index during 1981 to 1999. *Journal of Geophysical Research*, 106(D17): 20069-20083.

Zhu, K., and Wan, M., 1963. A productive science – Phenology, *Public Science (Chinese)*, No 1.
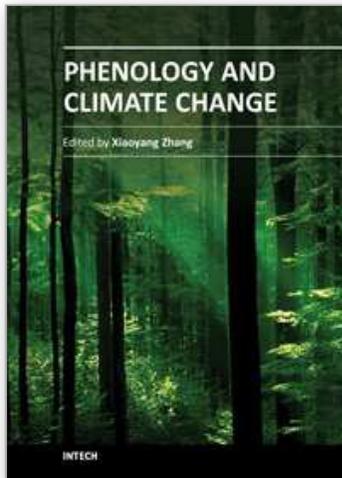
Phenology and Climate Change
Edited by Dr. Xiaoyang Zhang

ISBN 978-953-51-0336-3
Hard cover, 320 pages
Publisher InTech
Published online 21, March, 2012
Published in print edition March, 2012

Phenology, a study of animal and plant life cycle, is one of the most obvious and direct phenomena on our planet. The timing of phenological events provides vital information for climate change investigation, natural resource management, carbon sequence analysis, and crop and forest growth monitoring. This book summarizes recent progresses in the understanding of seasonal variation in animals and plants and its correlations to climate variables. With the contributions of phenological scientists worldwide, this book is subdivided into sixteen chapters and sorted in four parts: animal life cycle, plant seasonality, phenology in fruit plants, and remote sensing phenology. The chapters of this book offer a broad overview of phenology observations and climate impacts. Hopefully this book will stimulate further developments in relation to phenology monitoring, modeling and predicting.

INTECH
open science | open minds